IEEE Access
Multidisciplinary | Rapid Review | Open Access Journal

Received June 1, 2022, accepted June 13, 2022, date of publication June 16, 2022, date of current version June 22, 2022.

Digital Object Identifier 10.1109/ACCESS.2022.3183579

Low Loss W-Band Packaged Filtering Balun Based on a Modified Quarter-Mode Folded Substrate-Integrated Waveguide Cavity

LIXUE YANG, YANG YUAN, AND LIANG ZHOU, (Senior Member, IEEE)
Key Laboratory of Ministry of Education of Design and Electromagnetic Compatibility of High-Speed Electronic Systems, Shanghai Jiao Tong University, Shanghai 200240, China

Corresponding author: Liang Zhou (liangzhou@sjtu.edu.cn)

This work was in part supported by Guangdong Provincial Key-Field Research Program 2018B010115001, in part by the National Key Research and Development Project 2020YFB1804904, in part by National Natural Science Foundation of China 62188102, 61831016 and 61822112, in part by the Shanghai Science and Technology Commission under Grant 19511131800, and in part by Shanghai Aerospace Advanced Technology Joint Research Funding Project USCAST2019-21.

ABSTRACT A novel packaged filtering balun is proposed by modifying quarter-mode edge and diagonally folded SIW (FSIW) cavities. The TM_{220} mode is selected to realize the differential signal conversion by using a quarter-mode diagonally FSIW. Furthermore, TM_{130}, and TM_{330} modes are obtained by using a quarter-mode edge FSIW cavity by analyzing the mode field distributions. A W band packaged filtering balun is designed and simulated. Then, it is fabricated with 70 um thickness per layer based on our in-house Si-based MEMS photosensitive film process. The size of the filtering balun is only 2.83 λg^2 with insertion loss of 3 + 1.8 dB. These types of packaged filtering balun are very suitable for future 3D heterogeneous integration with other semiconductor devices.

INDEX TERMS Packaged, filtering balun, quarter-mode folded substrate-integrated waveguide, BCB, transmission zeros.

I. INTRODUCTION

A component that realizes the conversion between unbalanced and balanced ports, plays an important role in a millimeter wave communication system. Filtering balun not only provides the function of suppressing common mode signals to obtain differential feeds but also offers signal transmission in the passband and attenuation characteristics in the stopband. Often, the filtering balun needs to be compatible with the packaging technology, which is characterized by easy integration, planarization, and small volume.

Traditional filtering baluns are generally based on Marchand balun [1], [2]. They may have some advantages in bandwidth, but their insertion loss is usually large [3]–[5], especially in the millimeter-wave band. Substrate integrated waveguide has its advantages of low loss at millimeter wave, high power handling capability, and compatibility with planar circuits. The design of the filtering balun in a substrate integrated waveguide relied on the application of the cavity mode which produced phase difference of 180° [6]–[8]. However, to the best of our knowledge, most of the filtering balun based on mircostrip techniques were operated in microwave band. Few study have demonstrated in a quarter-mode folded SIW (FSIW) cavity in millimeter wave. Quarter-mode FSIW offers the advantages of less spurious modes and at least 75% size reduction compared with standard SIW cavity.

In this paper, a multi-layer packaged filtering balun is proposed by modifying a quarter-mode FSIW cavity, thereby making its size more compact than those of many other designs. The modes where quarter-mode edge and diagonally FSIW cavities can be precisely controlled are investigated. The W-band multilayer filtering balun was fabricated by adopting benzocyclobutene (BCB) as dielectrics. BCB is a photosensitive polymer that offers the advantages of a low dissipation factor and a low dielectric constant. The fabrication method for larger BCB thickness has been investigated to improve the quality factor of the cavity, which will result in lower insertion loss. In addition, it is very suitable for millimeter-wave and terahertz interconnections [9]. Therefore, the multi-layer filtering balun will have lower

The associate editor coordinating the review of this manuscript and approving it for publication was Mohammad Alshabi.

insertion loss and can be further interconnected and integrated with other active devices to obtain three-dimensional integration [10].

This paper is organized as follows. Section II demonstrates the realization of the proposed multi-mode resonator with quarter-mode FSIW cavity. Section III presents an example of the filtering balun design. Section IV describes the fabrication process. Section V illustrates the measurement results and tolerance analysis. Section VI concludes the study.

II. MODE ANALYSIS OF THE QUARTER-MODE FSIW

Two types of the quarter-mode FSIW can be obtained by edge and diagonal folding, as shown in Figs. 1 (a) and (b), respectively. Figs. 1 (c) and (d) show the top view of the quarter-mode edge and diagonal FSIW, respectively. For a quarter-mode edge FSIW cavity, a and b are the side lengths. In the following design, we set $a = b$.

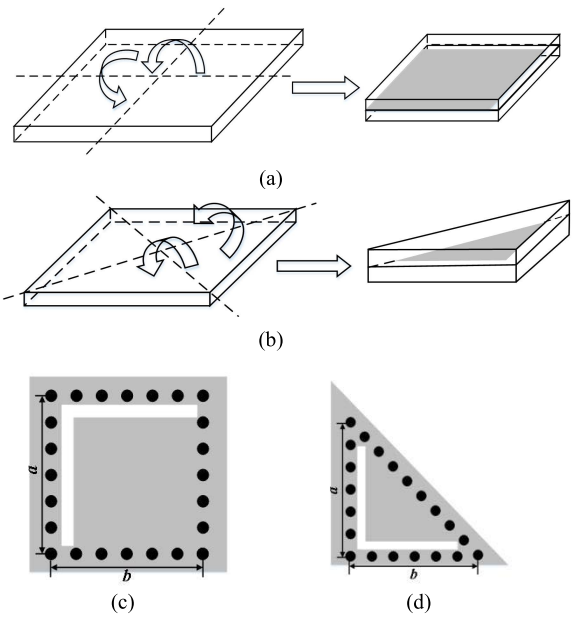

FIGURE 1. Quarter-mode FSIW (a) Edge folding, (b) diagonal folding, (c) top view of the edge folding, and (d) top view of the diagonal folding.

The boundary conditions of a quarter-mode edge FSIW cavity and their solutions of TM_{mn0} modes were presented in [5]. The eigenmode frequency in Fig. 1 satisfies:

$$f_{mn0} = \frac{c}{2\pi\sqrt{\mu_r\varepsilon_r}}\sqrt{\left(\frac{m\pi}{2a}\right)^2 + \left(\frac{n\pi}{2b}\right)^2} \quad (1)$$

where $m, n = 1, 3, 5\ldots$.

The modes in the following context are unified into a full-mode SIW cavity with a dimension of $2a \times 2b$.

The electric field distributions of the first five modes for the quarter-mode edge FSIW cavity are shown in Figs. 2 (a)–(e).

TE_{130} and TE_{310} are degenerated modes where the quality factor is higher than TE_{110}. We modified the quarter-mode edge FSIW cavity to control the degenerated modes. Fig. 3 (a) shows the structure wherein a grounded metal wall

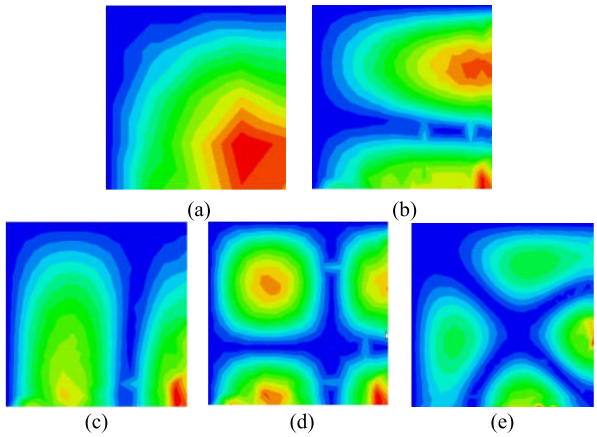

FIGURE 2. Electric field distributions of the first five modes for the quarter-mode edge FSIW cavity (a) TE110 (b) TE130 (c) TE310 (d) TE330 (e) TE510.

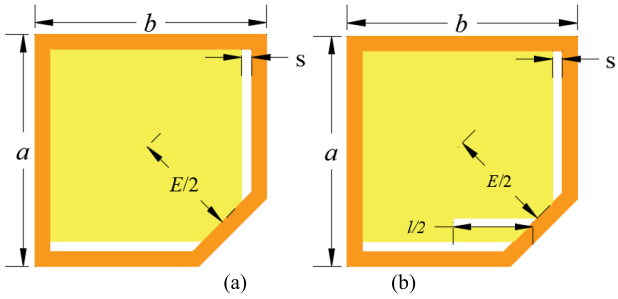

FIGURE 3. Structure of the modified quarter-mode edge FSIW (a) metal wall at the open apex (b) Slot line loaded at the open apex.

TABLE 1. Eigen-Mode and resonant frequency.

Serial number of modes	Modes (TE_{mn0})	Quarter-mode edge FSIW	Modified quarter-mode edge FSIW, as shown in Fig. 3 (a)
1	110	0.33	0.47
2	310	0.71	0.68
3	130	0.71	0.84
4	330	1	0.94

is introduced in the open-circuit vertex of the quarter-mode edge FSIW resonator where a, b, and s are 2 mm,2 mm and 0.1 mm, respectively. E/2 is the distance between the grounded metal wall and the center of the quarter-mode edge FSIW cavity. Fig. 4 shows the relationship between normalized frequency and E/2 for the different modes of the quarter-mode edge FSIW resonator when only a grounded metal wall is introduced. Revised f_4 (TE_{330}) is the ratio between the resonance frequency (TE_{330}) with metal wall at the open apex and the original resonance frequency (TE_{330}) without metal wall at the open apex. It can be found that revised f_4 (TE_{330}) is decreasing when E/2 is increasing. The degenerate modes TE_{130} and TE_{310} can be separated if we decrease E. When E $\leq$ 2 mm, the grounded metal wall will not much affect the degenerated modes where the curves become flat.

Therefore, E = 2 mm can be used as an initial value for design optimization. Table 1 presents the normalized frequency for the modified quarter-mode edge FSIW.

The frequency gap between TE_{130} and TE_{330} mode is approximately 1.2 times when E = 2 mm. A slot line is loaded to tune the TE_{330} mode. It is at the midpoint of the metal wall and is parallel to the edge of the quarter-mode edge FSIW, as shown in Fig. 3 (b). Fig. 5 shows the electric field distributions of TE_{130} and TE_{330} after loading the slot line.

Fig. 6 shows the normalized frequency of each mode for the quarter-mode edge FSIW versus L/2 where E is set to 2 mm. TE_{330} mode move toward TE_{130} and TE_{310} by increasing parameter L. When L is 1.94 mm, the frequencies of $TE_{130}$and TE_{330} are getting close. The frequencies of TE_{310} and TE_{130}, as well as the fundamental mode of TE_{110}, increase when L is smaller than 1.94 mm. On the contrary, they decrease if L is larger than 1.94 mm. The fundamental mode TE_{110} is about 1.5 and 1.9 times lower than TE_{310} and TE_{130} when L is 1.94 mm because TE_{110} increases slower than TE_{310} and TE_{130}. Therefore, quarter-mode edge folded FSIW has good suppression if we use TE_{130}, and TE_{330} to design a balun.

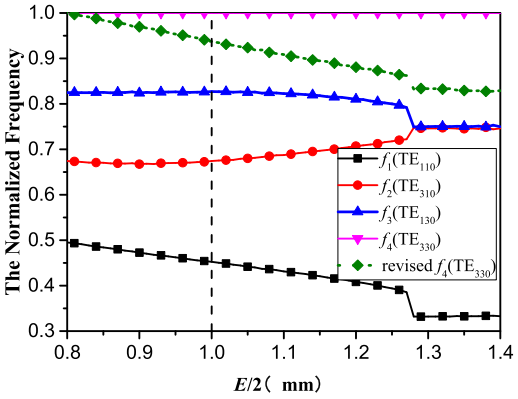

FIGURE 4. Normalized frequency of each mode for the modified quarter-mode edge FSIW versus E/2.

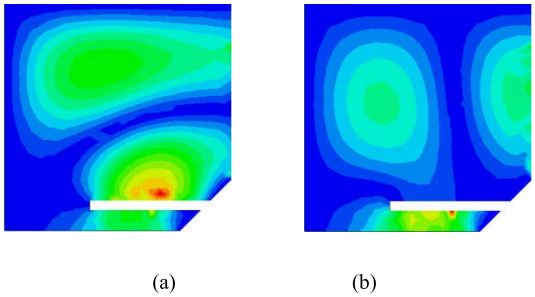

FIGURE 5. Electric field distributions of TE130 and TE330 of the modified quarter-mode edge FSIW with slot line (a) TE130 (b) TE330.

The electric field distributions of the quarter-mode diagonally FSIW cavity can also be plotted. Fig. 7 shows the first three modes. The TE_{220} mode provides the possibility for balun's design because the electric fields on both sides are equal in intensity and opposite in direction. If we set the appropriate dimensions of a and b in Fig. 1 (d), then the frequency of TE_{220} can operate at 90.43 GHz, whereas TE_{110} and TE_{130} are at 44.86 GHz and 100.91 GHz, respectively. The resonant frequency of TE_{130} is 1.17 times of TE_{220}. Therefore, suppression should be considered.

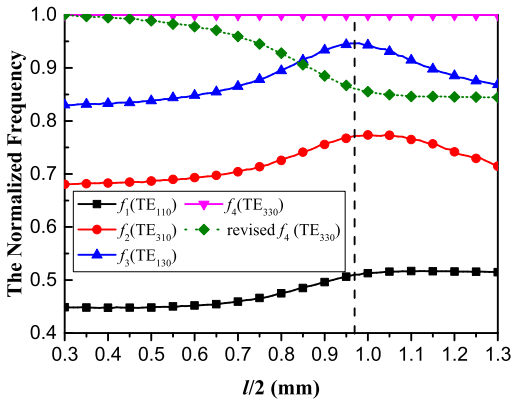

FIGURE 6. Normalized frequency of each mode for the modified quarter-mode edge FSIW versus L/2 where E is set to 2 mm.

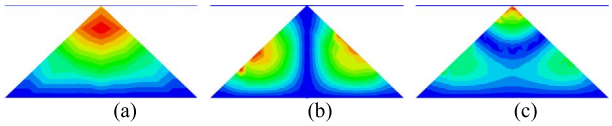

FIGURE 7. Electric field distributions of the quarter-mode diagonally FSIW, (a) TE110 at 44.86 GHz (b) TE220 at 90.43 GHz (c) TE130 at 100.91 GHz.

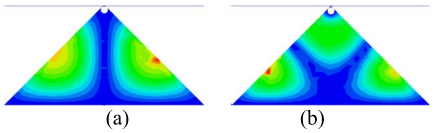

FIGURE 8. Electric field distributions of the modified quarter-mode diagonally FSIW with a grounded via, (a) TE220 (91.23 GHz) (b) TE130 (120.27 GHz).

A grounded via is placed at the vertex of the quarter-mode diagonally FSIW to move TE_{130} mode away from TE_{220} mode. Fig. 8 shows the electric field distributions of the modified quarter-mode diagonally FSIW with a grounded via. Table 2 presents the comparisons of the normalized frequency. TE_{220} has less influence by setting a ground via while the normalized resonant frequency of TE_{130} has increased from 1.17 times to 1.31 times.

III. FILTERING BALUN DESIGN EXAMPLE USING QUARTER-MODE FSIW

A W-band filtering balun with a center frequency f_0 at 92 GHz and a fractional bandwidth (FBW) of 3.3 % is designed using the proposed quarter-mode FSIW. Fig. 9 (a) shows the structure of the filtering balun. It consists of a balun

TABLE 2. Eigen-Mode and resonant frequency.

Serial number of modes	Modes (TE_{mn0})	Triangular DFSIW cavity	Modified triangular DFSIW cavity
1	110	0.49	0.73
2	220	1	1
3	130	1.17	1.31

and two multimode resonators. Fig. 9 (b) shows the topology with coupled balance ports. Particle swarm optimization algorithm [11] is used to synthesize the coupling matrix of a third-order filtering balun. According to the symmetry of filtering balun topology, it can be concluded that:

$$M'_{12} = -M'_{14}, M'_{13} = -M'_{15}, M'_{22} = M'_{44},$$
$$M'_{33} = M'_{55}, M'_{2L-} = M'_{4L+}, M'_{3L-} = M'_{5L+} \quad (2)$$

where the positive and negative signs of the coupling coefficient are according to the direction of the electric fields.

Through the above relationship, the degree of freedom of the adjacency matrix can be reduced, which reduces the convergence time of the algorithm to a certain extent. We improve the objective function [12] to form an objective function suitable for the extraction of coupling matrix of filtering balun:

$$K = \sum_{i=1}^{N} \left|S_{11}(\omega'_{zi})\right|^2 + \sum_{p=1}^{P} \left|S_{21}(\omega'_{pi})\right|^2 + \sum_{q=1}^{Q} \left|S_{31}(\omega'_{qi})\right|^2 \left(\left|S_{11}(\omega' = -1)\right| - \frac{\varepsilon}{\sqrt{1+\varepsilon^2}}\right)^2 + \left(\left|S_{11}(\omega' = 1)\right| - \frac{\varepsilon}{\sqrt{1+\varepsilon^2}}\right)^2 \quad (3)$$

where ω'_{zi} and ω'_{pi} represent the zeros and poles of the filter function, respectively. The S parameters of filtering balun corresponding to symmetrical topology should meet the following requirements:

$$S_{21} = -S_{31} \quad (4)$$

Therefore, Equation (3) can be simplified to:

$$K = \sum_{i=1}^{N} \left|S_{11}(\omega'_{zi})\right|^2 + 2 \times \sum_{p=1}^{P} \left|S_{21}(\omega'_{pi})\right|^2 + \left(\left|S_{11}(\omega' = -1)\right| - \frac{\varepsilon}{\sqrt{1+\varepsilon^2}}\right)^2 + \left(\left|S_{11}(\omega' = 1)\right| - \frac{\varepsilon}{\sqrt{1+\varepsilon^2}}\right)^2 \quad (5)$$

The coupling matrix is shown in Fig. 10 where a third-order filter response is designed with a transmission zero at 89 GHz, the in-band return loss is less than -20 dB. Fig. 11 shows the idea response of the proposed filtering balun, where the coupling matrix synthesis results show agreements with the simulated results and M12 and M13 are opposite according to the direction of the electric fields.

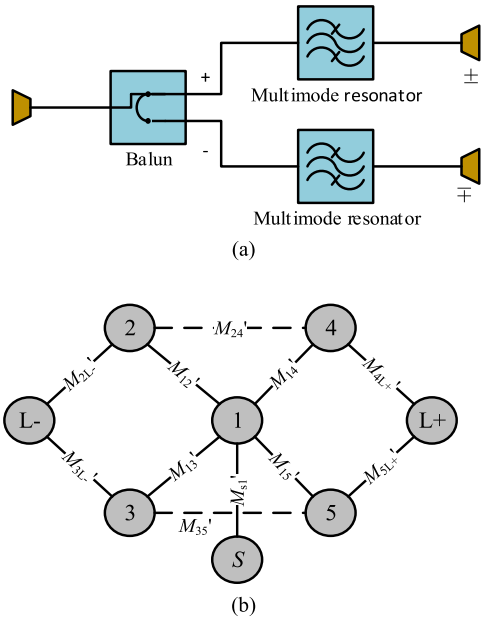

FIGURE 9. Proposed filtering balun, (a) structure (b) Topology.

$$\begin{bmatrix} 0 & 1.1757 & 0 & 0 & 0 & 0 & 0 & 0 \\ 1.1757 & -0.0805 & -0.3053 & 0.8120 & 0.3053 & -0.8120 & 0 & 0 \\ 0 & -0.3053 & 0.8878 & 0 & -0.3960 & 0 & 0.6382 & 0 \\ 0 & 0.8120 & 0 & -0.4394 & 0 & 0.3834 & 1.0053 & 0 \\ 0 & 0.3053 & -0.3960 & 0 & 0.8878 & 0 & 0 & 0.6382 \\ 0 & -0.8120 & 0 & 0.3834 & 0 & -0.4394 & 0 & 1.0053 \\ 0 & 0 & 0.6382 & 1.0053 & 0 & 0 & 0 & 0 \\ 0 & 0 & 0 & 0 & 0.6382 & 1.0053 & 0 & 0 \end{bmatrix}$$

FIGURE 10. Coupling matrix of the proposed filtering balun.

The structure of the proposed filtering balun is mainly composed of a modified quarter-mode diagonally FSIW cavity (a balun) and two modified quarter-mode edge FSIW cavities (multimode resonators), as shown in Fig. 12. The quarter-mode diagonally FSIW cavity operates at TE_{220} as resonator 1, as shown in Fig. 9. The modified quarter-mode edge FSIW cavities operate at TE_{130} and TE_{330} as resonators 2, 3, and 4, 5 as shown in Fig. 9. The coupling coefficient of the cavities can be calculated from Equation (6).

$$k_{ij} = \pm\frac{1}{2}\left(\frac{f_{0j}}{f_{0i}} + \frac{f_{0i}}{f_{0j}}\right)\sqrt{\left(\frac{f_j^2 - f_i^2}{f_j^2 + f_i^2}\right)^2 - \left(\frac{f_{0j}^2 - f_{0i}^2}{f_{0j}^2 + f_{0i}^2}\right)^2} \quad (6)$$

where f_{0i} and f_{0j} represent the resonance frequency of different resonators. When $f_{0i} = f_{0j}$, we will have

$$k_{\mathrm{ij}} = \pm\frac{f_{\mathrm{j}}^2 - f_{\mathrm{i}}^2}{f_{\mathrm{j}}^2 + f_{\mathrm{i}}^2} \quad (7)$$

Striplines are used as the coupling structures between the modified quarter-mode diagonally FSIW cavity and two modified quarter-mode edge FSIW cavities. The maximum coupling coefficient can be obtained as the electric field

distributions of the modified quarter-mode diagonally FSIW cavity (a balun) and is strongest at the midpoint of its left and right-angle edges, as shown in Fig. 8 (a). Fig. 13 shows the coupling coefficient versus parameter t between the edge and diagonally FSIW cavities. The initial value of t is set to 0.1 mm based on the coupling coefficient of the matrix.

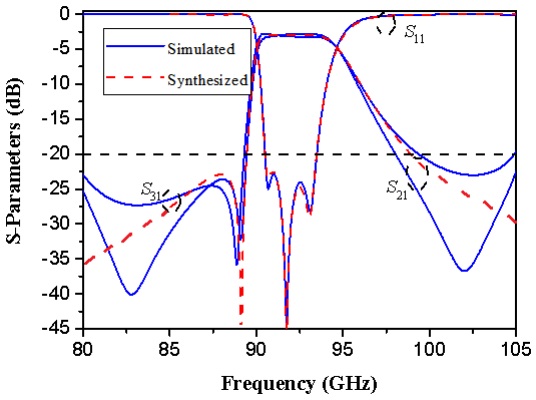

FIGURE 11. Idea response of the proposed filtering balun.

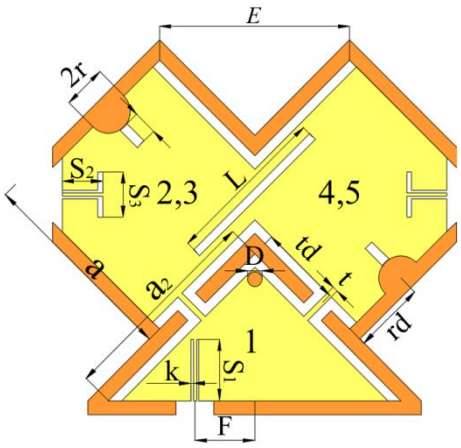

FIGURE 12. Proposed structure of the filtering balun.

The two modified quarter-mode edge FSIW cavities are coupled through their metal walls, which are equivalent to the electric wall. The coupling coefficient can be modified by varying the distance (E) between the cavities. Fig. 14 shows the coupling coefficient versus the distance (E) when a and b are set to 2 mm. The coupling coefficient between the cavities decreases gradually when the distance (E) increases. Based on the coupling coefficient of the matrix, the initial distance (E) is set to 2 mm at 92 GHz and then optimized by using full-wave simulation to obtain its final value.

Fig. 15 (a) show the external quality factor (Q_{e1}) versus parameters (S_1), and (F) at the input of the filtering balun. Q_{e1} decreases with the increase in S_1 and F. However, the decreasing rate of Q_{e1} becomes smaller if S_1 increases, indicating that the suitable value of Q_e can be obtained by selecting the appropriate parameters of S_1 and F from the coupling

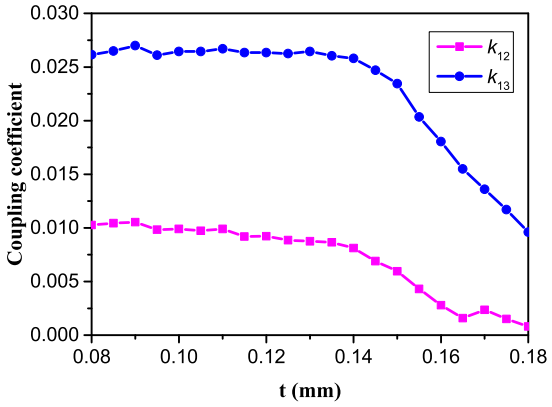

FIGURE 13. Coupling coefficient versus t between the edge and diagonally FSIW cavities.

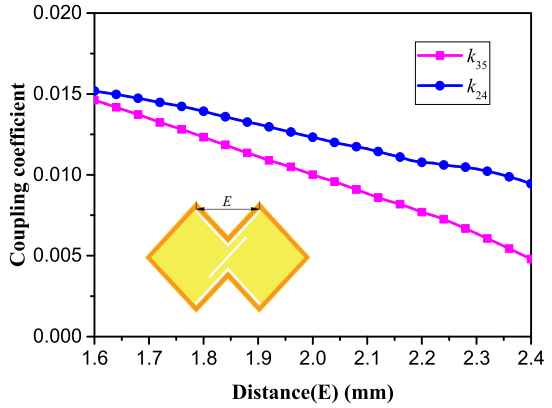

FIGURE 14. Coupling coefficient versus the distance (E) between cavity where a and b are set to 2 mm.

matrix. Fig. 15 (b) shows the external quality factor Q_{e2} and Q_{e3} versus parameters (S_2) at the output of the filtering balun.

Q_e can be calculated by equations (8) and (9), where Q_{e1} is 22.19, and S_1 and F are set to 0.65 mm at 92 GHz as the initial value before optimization, respectively. Q_{e2} and Q_{e3} are 30.18 and 75.3, respectively. S_2 is set to 0.47 mm.

$$M_{s1} = \sqrt{\frac{1}{Q_{e1}FBW}} \tag{8}$$

$$M_{Li} = \sqrt{\frac{1}{Q_{ei}FBW}} \tag{9}$$

Based on the topology and structure of the filtering balun, a transmission zero is generated on the left side of the passband, which improves frequency selectivity. A semi-cylinder is designed on the side wall of the modified quarter-mode edge FSIW to control the position of the transmission zero flexibly. The transmission zero is controlled by the radius (r) of the semi-cylinder (Fig. 12).

Fig. 16 shows the S parameter of the filtering balun under weak external coupling excitation. The transmission zero can be controlled by varying radius r. Fig. 17 shows the normalized resonance frequency of each mode versus the radius (r)

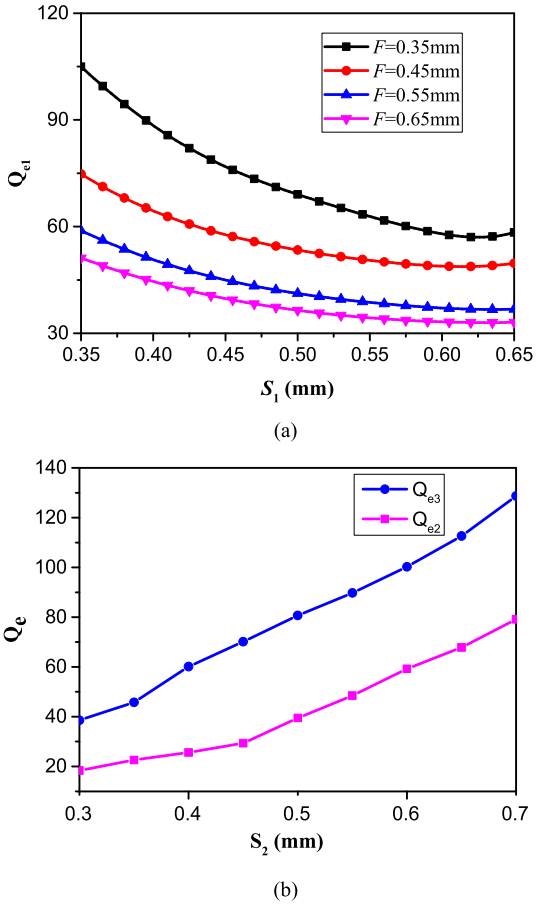

FIGURE 15. Q_e versus (a) parameters S_1 and F, (b) parameter S_2 where the input and output impedance are 50 Ω.

of the modified quarter-mode edge FSIW, where rd is set to 0.77 mm. The semi-circle grounded via has less influence for the frequency of the cavities, except the transmission zero of the filtering balun.

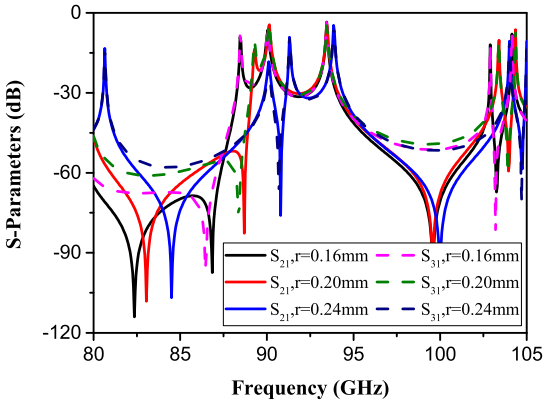

FIGURE 16. S-parameters of a filtering balun under weak external coupling excitation.

IV. FABRICATION OF THE FILTERING BALUN

Fig. 18 (a) shows the multilayer structures of the proposed multilayer filtering balun, which is fabricated on a silicon wafer. With MEMS technology, BCB polymer

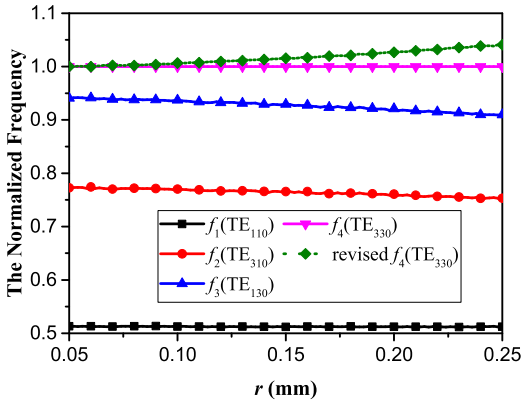

FIGURE 17. Normalized resonance frequency of each mode verses radius (r) of the modified quarter-mode edge FSIW where rd is set to 0.75 mm.

(CYCLOTENE 4026-46) is utilized as dielectrics. It has a dielectric constant of 2.65 and a low dissipation factor of 0.0008. The permeability is 1. Table 3 listed the design parameters.

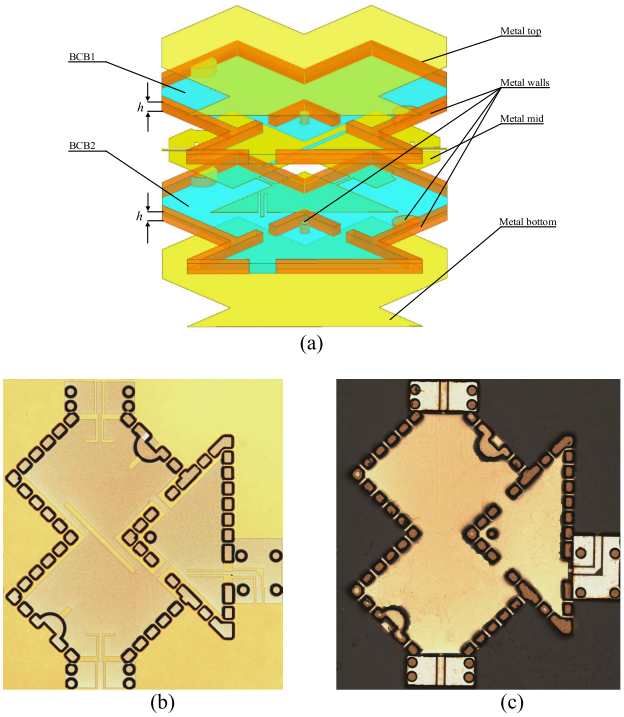

FIGURE 18. (a) Structures of the proposed multilayer filtering balun. (b) Photo of the proposed multilayer filtering balun without the top metal plane. (c) Photo of the packaged multilayer filtering balun. The dissipation factor of the BCB is 0.0008 and the dielectric constant is 2.65.

Two layers of dielectric, each with a thickness of 70 μm are fabricated to enhance the quality factor of the filtering balun. In our process, cavities are etched in the silicon substrate, which is the half of the filtering balun. The thickness of one-layer BCB is deposited in the cavities. This method reduces the degree of surface warping and improves the fabrication yields. In addition, because of many regular-arranged vias in this SIW based filtering balun, a new fabrication method of

TABLE 3. Design Parameters in Fig. 11 (Unit: mm).

a	1.994	r	0.241	S_1	0.05
b	1.994	t	0.097	F	0.62
l	1.69	D	0.075	k	0.04
a_2	2.324	S_2	0.5	E	2.05
rd	0.77	h	0.07	t_d	0.73
S_3	0.22	S_4	0.054	l_k	0.08

silicon-based pillars with metallized surface, which help to reduce the fabrication difficulties and improve its accuracy, are investigated.

Fig. 19 illustrates the fabrication process. A 50 Ω thin film resistor [13] is also fabricated in the multilayer packaged filtering balun because of difficulties in three port millimeter wave measurements. Therefore, two filtering baluns are fabricated, one 50 Ω thin film resistor is terminated in the third ports when S_{21} is measured, by the contrast, one 50 Ω thin film resistor is terminated in the second ports, when S_{21} is measured.

1) A 1000 μm thickness high resistivity silicon wafer is used as a substrate, as shown in Fig. 19 (a).
2) Vertical cavities and silicon-based pillars are etched using BOSCH process with photoresist protection, as shown in Fig. 19 (b).
3) A thin-film resistor (50 Ω) is fabricated by using sputtering, photolithography, and etching [13], as shown in Figs. 19 (c)–(e).
4) A layer of negative photoresist (5300) is spread, and photolithographic development is carried out for the graphic of metal layers, as shown in Fig. 19 (f).
5) A seed layer is then sputtered, and 4 μm copper is then electroplated, as shown in Fig. 19 (g).
6) Silicon-based pillars and the transfer of the metal layer pattern are completed after the wafer soaked in acetone for several minutes, the copper is then peeled off along with the photoresist 5300, as shown in Fig. 19 (h).
7) BCB is then spin coated several times until the BCB in the cavities is higher than the surface, as shown in Fig. 19 (I).
8) Mechanical polishing is then used to make the surface flat where the BCB is the same level of the silicon surface, as shown in Fig. 19 (j).
9) The electrode of the thin-film resistance is then exposed after a thin layer of BCB is spin coated and developed, as shown in Fig. 19 (k).
10) The second seed layer is then sputtered with patterns created, and metal layers are fabricated by electroplating and ion beam etching, as shown in Fig. 19 (l).
11) BCB is then spin coated several times to develop another 70 um thickness, as shown in Fig. 19 (m).
12) The third metal layer is then developed after sputtering, photolithography, electroplating, and ion beam etching, as shown in Fig. 19 (n).

V. EXPERIMENTAL RESULTS AND DISCUSSION

The measured stage consists of a Keysight 5247A network analyzer, two Keysight N5250CX10 frequency extender

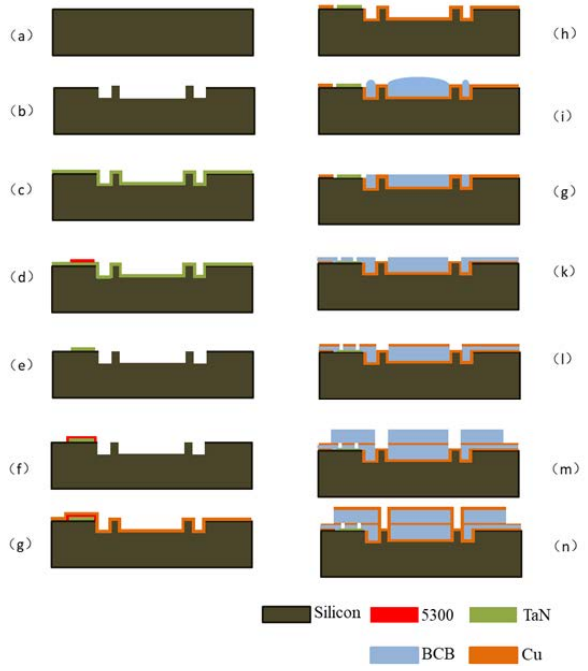

FIGURE 19. Fabrication of the filtering balun. (a) 1000 μm thickness high resistivity silicon wafer, (b) Vertical cavities and silicon-based pillars are etched, (c) - (e) thin-film resistor (50 Ω) is fabricated, (f) One layer of negative photoresist (5300) is spread, (g) 4 μm copper is then electroplated, (h) Silicon-based pillars and the transfer of the metal layer pattern are completed, (I) BCB is then spin coated, (j) Mechanical polishing, (k) electrode of the thin-film resistance is exposed, (l) the second seed layer is then sputtered, (m) BCB is spin coated, (n) the third metal layer is then developed.

modules, two Cascade GSG probes (I100-AM-GSG-100), a Cascade E300 probe station, and some accessories. This stage supports the measured frequency range from DC to 110 GHz. The photo of the measurement setup is shown in Fig. 20. Fig. 21 shows the simulated and measured S-parameter of the filtering balun where one of the output ports are terminated by a 50 Ω thin film resistor. The measurement shifts approximately 1.1 GHz with the minimum insertion loss 3+1.8 dB, which is 0.9 dB higher than the simulated results. The out-of-band suppression of transmission zero is about 40 dB at 91 GHz, which is 1.18 GHz offset compared with the simulated results. Fig. 22 shows the simulated and measured amplitude and phase imbalance of the filtering balun. The measurement results are focused on their imbalance of 91.9–95.6 GHz because of the frequency deviation. The overall measured amplitude imbalance is less than 0.9 dB with the phase imbalance less than 10°. The measured amplitude and phase imbalance have differences of 0.4 dB and 3° compare to the simulated results. Table 4 shows the comparisons between our proposed filtering balun and other works. Our proposed work has advantages in insertion loss and size.

The tolerance of the fabrication is important for the development of a real filtering balun. These factors often cause the frequency shift between the simulated and measured results. For example, the fabricated filtering balun in Fig. 19 has

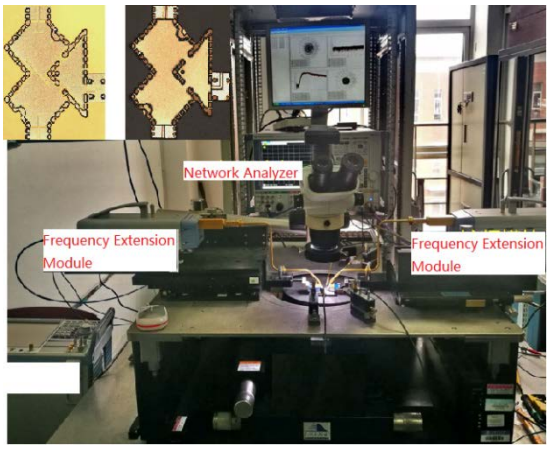

FIGURE 20. Photo of the measurement setup.

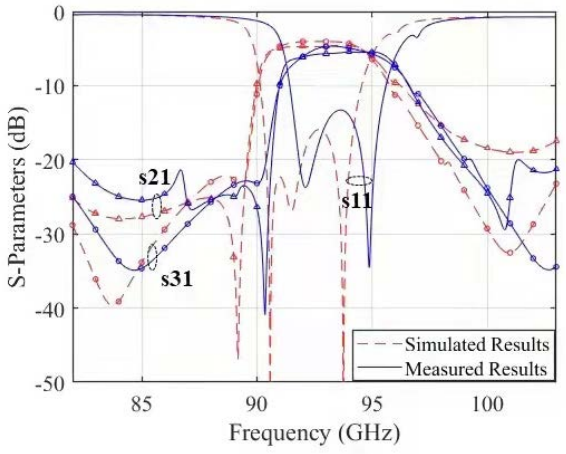

FIGURE 21. Simulated and measured S-parameter of the filtering balun.

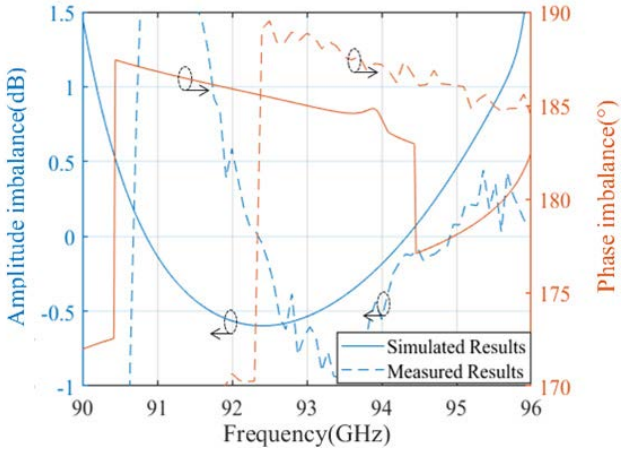

FIGURE 22. Simulated and measured amplitude and phase imbalance of the filtering balun.

a center frequency shift of 1.1 GHz. The main reason for this shift is the fabrication inaccuracies. We mainly focus on the tolerance analysis of key dimension parameters where frequency shift might occur was carried out by HFSS in order

TABLE 4. Comparisons between our proposed filtering balun and other works.

Ref.	order	f_0 (GHz)	FBW (%)	IL (dB)	IM(dB) / PM(°)	Fabric	Size (λ_g^2)
[3]	4	59.6	3	3+3.5	1.1/3.4	LTCC	7.15
[4]	2	77	18	3+3	1.4/4	CMOS	0.19
[5]	2	29.2	3.76	3+2.5	1/5	PCB	4
[6]	5	10.46	5.7	3+1.4	1.5/3	PCB	6.14
[7]	/	8.9	4.76	/	/	PCB	0.79
[8]	2/1	9/ 9.8	1.11/ 1.22	3+1.8	0.6/2	PCB	2.30
[14]	/	3.5	21	3+1.9	0.3/3	PCB	0.06
[15]	2	5.5	3.6	3+1	0.16/2	PCB	/
[16]	2	2.78	23.4	3+1.2	0.5/5	PCB	0.07
[17]	2	3.4	10	3+1.8	0.5/3	LTCC	0.01
This work	3	92	3.26	3+1.8	0.9/10	MEMS	2.83

to accurately predict the influence of different machining errors on the filter. Figs. 23 (a)–(c) show the insertion loss of the filtering balun versus the length (L), width (L_k) of the slot line and electroplating thickness (d_r).

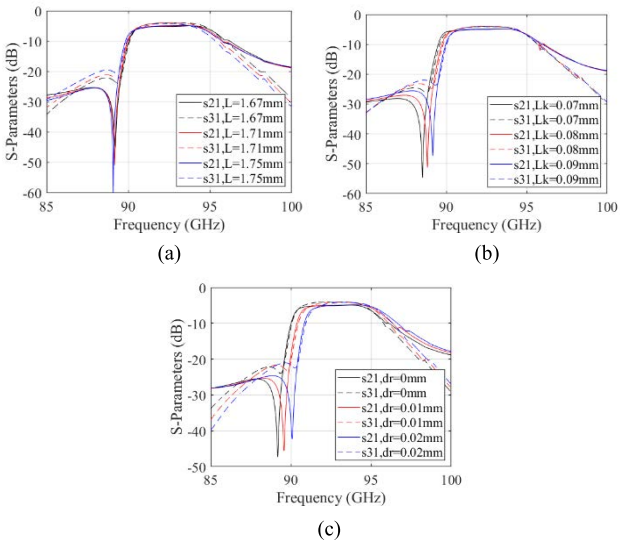

FIGURE 23. Fabrication tolerance analysis of the filtering balun, (a) Parameter (L) versus frequency, (b) Parameter (Lk) versus frequency, (c) Parameter (dr) versus frequency.

The electroplating thickness (dr) has impact to the frequency offset, but has less influence to the insertion loss and imbalance. For example, if the thickness increases to 10 μm, the frequency shifts about 0.37 GHz because the electroplating uniformly wraps a layer of copper on silicon-based pillars,

and the diameter of the silicon-based pillars with metallized surface increases with the electroplating thickness. Therefore, the resonance cavity decreases when the resonant frequency increases.

The length (L) of the slot line will affect TM_{330} mode, if it is smaller than the designed value, then the frequency of TM_{330} mode will be higher, which will result in increase in the operating frequency of the filtering balun. In addition, if the width (L_k) of the slot line increases due to the increase in equivalent inductance, the center frequency of the filtering balun also shifts higher.

VI. CONCLUSION

In this paper, two types of modified quarter-mode FSIW have been analyzed and designed. A W band third-order multi-layer packaged filtering balun has been designed, simulated, and measured on the basis of these two types of FSIW. One layer 70 um thickness of BCB has been investigated with two layers has been achieved to obtain a low loss filtering balun based on our in-house MEMS fabrication process. The measured insertion loss of the filtering balun is 3+1.8 dB with a comparable small size. These types of packaged filtering balun are very suitable for the future 3D heterogeneous integration with other semiconductor devices.

REFERENCES

[1] C. Cai, J. Wang, L. Zhu, and W. Wu, "A new approach to design microstrip wideband balun bandpass filter," *IEEE Microw. Wireless Compon. Lett.*, vol. 26, no. 2, pp. 116–118, Feb. 2016.

[2] J.-X. Xu, X. Y. Zhang, and X.-L. Zhao, "Compact LTCC balun with bandpass response based on Marchand balun," *IEEE Microw. Wireless Compon. Lett.*, vol. 26, no. 7, pp. 493–495, Jul. 2016.

[3] G. Zhang, J. Wang, J. Pan, and H. Gu, "Compact 60 GHz LTCC balun bandpass filter with two transmission zeroes," *Electron. Lett.*, vol. 51, no. 8, pp. 637–638, Apr. 2015.

[4] C.-Y. Hsu, C.-Y. Chen, and H.-R. Chuang, "A 77-GHz CMOS on-chip bandpass filter with balanced and unbalanced outputs," *IEEE Electron Device Lett.*, vol. 31, no. 11, pp. 1205–1207, Nov. 2010.

[5] X. F. Ye, H. Y. Ke, and S. Y. Zheng, "A millimeter-wave bandpass filter and balun filter based on circular sector patch," in *Proc. Int. Workshop Electromagnetics, Appl. Student Innov. Competition (iWEM)*, Nov. 2015, pp. 1–2.

[6] L.-S. Wu, Y.-X. Guo, J.-F. Mao, and W.-Y. Yin, "Design of a substrate integrated waveguide balun filter based on three-port coupled-resonator circuit model," *IEEE Microw. Wireless Compon. Lett.*, vol. 21, no. 5, pp. 252–254, May 2011.

[7] H.-Y. Li, X. L. Zhao, J.-X. Xu, X. Y. Zhang, and Z. H. Wu, "Novel compact substrate integrated waveguide balun filter and balanced filter," in *Proc. Int. Appl. Comput. Electromagn. Soc. Symp. China (ACES)*, Jul. 2018, pp. 1–2, doi: 10.23919/ACESS.2018.8669208.

[8] H. Chu and J.-X. Chen, "Dual-band substrate integrated waveguide balun bandpass filter with high selectivity," *IEEE Microw. Wireless Compon. Lett.*, vol. 24, no. 6, pp. 379–381, Jun. 2014.

[9] X.-L. Huang, L. Zhou, Y. Yuan, L.-F. Qiu, and J.-F. Mao, "Quintuple-mode W-band packaged filter based on a modified quarter-mode substrate-integrated waveguide cavity," *IEEE Trans. Compon., Packag., Manuf. Technol.*, vol. 9, no. 11, pp. 2237–2247, Nov. 2019.

[10] X. Yang, Y.-S. Huang, L. Zhou, Z. Zhao, D.-X. Ni, C.-R. Zhang, J.-F. Mao, J.-A. Han, X. Cheng, and X.-J. Deng, "Low-loss heterogeneous integrations with high output power radar applications at W-band," *IEEE J. Solid-State Circuits*, vol. 57, no. 6, pp. 1563–1577, Jun. 2022, doi: 10.1109/JSSC.2021.3106444.

[11] J. Kennedy and R. Eberhart, "Particle swarm optimization," in *Proc. Int. Conf. Neural Netw. (ICNN)*, Perth, WA, Australia, Nov. 1995, p. 1.

[12] S. Amari, "Synthesis of cross-coupled resonator filters using an analytical gradient-based optimization technique," *IEEE Trans. Microw. Theory Techn.*, vol. 48, no. 9, pp. 1559–1564, Sep. 2000, doi: 10.1109/22.869008.

[13] T.-T. Li, L. Zhou, and W.-Y. Yin, "Design, fabrication and measurement of TaN thin film resistor based on MEMS technology," in *Proc. Int. Conf. Microw. Millim. Wave Technol. (ICMMT)*, Shanghai, China, Sep. 2020, pp. 1–3.

[14] H. Chang, W. Sheng, and J. Cui, "Design of planar baluns with filtering response using coupled line sections," *IEEE Microw. Wireless Compon. Lett.*, vol. 31, no. 9, pp. 1035–1038, Sep. 2021, doi: 10.1109/LMWC.2021.3095504.

[15] X. Shen, W. Feng, H. Chen, and W. Che, "Narrowband filtering balun power divider based on SIW and CSRRs," in *Proc. Int. Conf. Microw. Millim. Wave Technol. (ICMMT)*, May 2018, pp. 1–3, doi: 10.1109/ICMMT.2018.8563701.

[16] H. Xu, J. Wang, L. Zhu, F. Huang, and W. Wu, "Design of a dual-mode balun bandpass filter with high selectivity," *IEEE Microw. Wireless Compon. Lett.*, vol. 28, no. 1, pp. 22–24, Jan. 2018, doi: 10.1109/LMWC.2017.2773040.

[17] D.-S. Wu, Y. C. Li, Q. Xue, W. Feng, and B.-J. Hu, "Synthesis and design of LTCC filtering balun with wide stopband," *IEEE Trans. Circuits Syst. II, Exp. Briefs*, vol. 67, no. 8, pp. 1404–1408, Aug. 2020, doi: 10.1109/TCSII.2019.2940112.

LIXUE YANG received the B.S. degree in electromagnetic field and microwave techniques from Xidian University, Xi'an, China, in 2019. She is currently pursuing the M.Sc. degree in electronic science and technology with Shanghai Jiao Tong University, Shanghai, China.

Her research interests include millimeter-wave integrated circuit and passive components design for 3-D heterogeneous integration applications.

YANG YUAN is currently pursuing the M.S. degree in electronic science and technology with Shanghai Jiao Tong University, Shanghai, China.

LIANG ZHOU (Senior Member, IEEE) received the Ph.D. degree in electrical engineering from the University of York, U.K., in 2005.

At York, he was working on ultra low phase noise oscillators. From 2005 to 2006, he was a Senior RF Engineer with Motorola Inc., Shanghai, China, where he involved in power amplifier design for the next generation of base station transceivers. He was a Visiting Scholar with the Massachusetts Institute of Technology, Cambridge, USA, in 2007. Since February 2017, he has been a Research Fellow with the Institute for Electronics Engineering (LTE), Friedrich-Alexander-University Erlangen-Nurnberg, Germany, granted by the Alexander von Humboldt-Stiftung. He is currently a Full Professor with the Key Laboratory of Ministry of Education of Design and Electromagnetic Compatibility of High-Speed Electronic Systems, Shanghai Jiao Tong University, Shanghai. His main research interests include system on packaging (SOP) design and modeling, EMC and high power microwave (HPM) protection of communication platforms, and multi-physics and its application.

Dr. Zhou was a recipient of the National Science Fund for Excellent Young Scholars, in 2018, the Alexander von Humboldt (AvH) Research Fellowship, in 2016, the APEMC Young Scientist Award, in 2016, the Research Grant of the Okawa Foundation, Japan, in 2016, the International Union of Radio Science (URSI) Young Scientist Award, in 2014, the Best Paper Awards of Cross Strait Quad-Regional Radio Wireless Conference (CSQRWC), in 2014, and the National Science and Technology Advancement Award of China, in 2012. He was the IEEE EMC Distinguished Lecturer (2019–2020). He is the IEEE EMC Shanghai Chapter Chair.